Neural correlates of imaging biomarkers for primary motor deficits after stroke – more than just the primary motor system?

Christoph Sperber, PhD, Johannes Rennig, PhD, Hans-Otto Karnath, MD, PhD

Center of Neurology, Division of Neuropsychology, Hertie-Institute for Clinical Brain Research, University of Tübingen, Tübingen

Corresponding Author:
Christoph Sperber
Center of Neurology
University of Tübingen
72076 Tübingen
Germany
e-mail: christoph.sperber@klinikum.uni-tuebingen.de

ABSTRACT

Background: Hemiparesis is a common consequence of stroke to the primary motor system. Brain mapping and post-stroke outcome prediction studies suggest that damage to additional brain areas plays a causal role in occurrence and severity of hemiparesis and its recovery.

Objective: The study aimed to evaluate if damage to areas outside of the primary motor system can play a causal role in the occurrence of hemiparesis, or if such brain-deficit relations constitute a mere correlation.

Methods: In a sample of 102 patients with unilateral stroke, the neural correlates of acute and chronic upper limb paresis were mapped by univariate and multivariate lesion behavior mapping. Following the same approach, CST lesion biomarkers were mapped, and resulting topographies of both analyses were compared.

Results: All mapping analyses of acute or chronic upper limb paresis implicated areas outside of the primary motor system. Likewise, mapping CST lesion biomarkers – that, by definition, are only causally related to damage of the CST – implicated several areas outside of the CST with high correspondence to areas associated with upper limb paresis.

Conclusions: Damage to areas outside of the primary motor system might not play a causal role in hemiparesis, while still providing predictive value. This finding suggests that simple theory-based biomarkers or qualitative rules to infer post-stroke outcome from imaging data might perform sub-optimally. Algorithms using theory-driven feature selection do not consider the complexity of lesion data, and could be improved by utilizing high-dimensional models with data-driven feature selection strategies.

INTRODUCTION

Brain lesions through strokes are a leading cause of acquired disability, and primary motor deficits are among its most common and debilitating symptoms. It is widely assumed that damage of the corticospinal tract (CST) underlies persisting primary motor deficits (Lindenberg et al., 2010; Lo et al., 2010; Zhu et al., 2010; Park et al., 2016). In conclusion, strategies to predict long-term motor outcome focused on assessing CST integrity by brain imaging (Lindenberg et al., 2010; Stinear et al., 2012; Wang et al., 2012; Sterr et al., 2014; Buch et al., 2016) or neurostimulation (Stinear et al., 2012).

Several studies developed prediction algorithms for motor outcome solely based on measures of CST damage derived from clinical CT or MR imaging (Wenzelburger et al., 2005; Zhu et al., 2010; Feng et al., 2015; Findlater et al., 2019). Metrics of CST lesion load were derived by referencing topographical lesion data to probabilistic topographies of the CST obtained by fiber tracking in healthy controls (Zhu et al., 2010; Feng et al., 2015; Findlater et al., 2019). These metrics were used in low-dimensional regression methods to predict motor outcome with moderate precision. However, two prediction studies using high-dimensional regression methods achieved better predictions when voxel-wise features were not only selected within the primary motor system, i.e. the CST and primary motor cortex, but, additionally, from a set of frontal, subcortical, and parietal areas (Rondina et al., 2016; Rondina et al., 2017). The authors hypothesized that integrity of these regions plays a role in both motor deficits and motor recovery for their relation to motor and sensory function according to the literature. In other words, they performed a theory-driven feature selection, which resulted in improved prediction performance. A similar study found that in patients with stroke not confined to subcortical areas, using features taken from outside the CST improves model quality (Park et al., 2016). These finding are complimentary to lesion-behavior mapping studies that found neural correlates of hemiparesis outside primary motor regions. Disintegrity of a cingulo-opercular attention control network was shown to contribute to motor deficits (Rinne et al., 2017). Association fibers, the insula, and perisilvian areas were found to be associated with primary motor deficits in right hemisphere stroke, underlining a possible role of right hemisphere brain networks in motor recovery (Frenkel-Teledo et al., 2019). Another study found putamen and several fiber tracts to be associated with poor motor outcome (Findlater et al., 2019). Taken together, these findings suggest that

stroke to regions outside the primary motor system contributes to primary motor deficits. The identification of such regions is of high relevance in motor outcome prediction, as it provides a foundation for feature selection.

A possible objection against the relevance of non-primary motor regions comes from critical discussions on lesion-deficit inference. Topographical results in lesion behavior mapping have been found to be biased by typical lesion anatomy (Mah et al., 2014; Sperber et al., 2019). It was postulated that the differentiation between areas where brain damage causes a deficit and areas where damage simply coincides with a deficit is impossible with current implementations of lesion-deficit inference (Sperber, 2020). Thus, strictly speaking, findings in previous studies might not be wrong, however, the causal interpretation of their role might be a misattributed. On the other hand, information outside of brain regions where damage causes a symptom could bear predictive value for a symptom (Sperber, 2020).

The present study aimed to re-evaluate the neural correlates of upper limb paresis in 102 stroke patients. We used lesion behavior mapping to identify regions associated with both acute and chronic upper limb paresis. We compared these topographies to regions associated with CST lesion biomarkers, which, per definition, are only causally related to damage to the CST. We hypothesized that mapping upper limb paresis should find areas outside the primary motor system, either because damage in these areas actually contributes in some way to primary motor deficits, or because damage coincides with damage to the primary motor system. Further, we hypothesized that CST lesion biomarkers will also be associated with regions outside the CST. Such finding would hint at brain areas where lesion-deficit associations are merely coincidental, which suggests that damage in these areas might not play any causal role for hemiparesis, while still bearing predictive value.

METHODS

Patient recruitment and motor assessment

Patients with a first unilateral cerebral stroke admitted to the Center of Neurology at the University of Tübingen were recruited. Diagnosis was confirmed by CT or MRI imaging. Patients with a medical history of other neurological or psychiatric disorders were excluded. All patients were re-examined in the chronic post-stroke stage at least 50 days and on average 423 days after the incident, and patients who suffered a second stroke were excluded. The final patient sample included 102 subjects (age =

59.9 years, SD = 13.0 years; 47 female, 55 male), of which 68 had stroke to the right, and 34 to the left hemisphere. The study has been performed in accordance with the standards laid down in the revised Declaration of Helsinki and patients or their relatives consented to the scientific use of the data.

Paresis of the upper limb was assessed by the BMRC (British Medical Research Council) scale on average 1.0 days (SD = 2.2 days) after stroke onset. The BMRC scoring ranges from zero to five (0: no movement, 1: palpable flicker, 2: movement without gravity, 3: movement against gravity 4: movement against resistance, 5: normal movement) and allows intermediate decimals in steps of 0.5. Ratings for distal and proximal upper limb motor function were averaged per patient.

Imaging and lesion delineation

Structural brain imaging was acquired by clinical CT or MRI on average 2.1 days (SD = 2.7 days) after stroke onset. If multiple scans were available, scans were chosen to be as acute as possible, while clearly depicting the borders of the lesion. If both suitable MRI and CT were available, MR scans were preferred. To visualize acute structural brain damage using MRI, diffusion weighted imaging was used in the first 48h after stroke onset, and T2 fluid attenuated inversion recovery imaging afterwards. If available, these images were co-registered with a high-resolution T1 MRI to be used in the normalization process.

Lesions were manually delineated on axial slices of the scans using MRIcron (https://www.nitrc.org/projects/mricron) by two experimenters, and the accuracy of lesion drawings was validated by consensus with the third experimenter. Scans were warped into 1x1x1 mm^3 MNI coordinates using age-specific templates in Clinical Toolbox (Rorden et al., 2012) and normalization algorithms in SPM 12 (www.fil.ion.ucl.ac.uk/spm), using cost-function masking to control for the lesioned area in the normalization process. The same normalization parameters were then applied to the lesion maps to obtain normalized binary lesion maps. Next, lesion maps of left hemisphere stroke patients were flipped along the sagittal mid-plane so that all lesions were depicted in the right hemisphere. This step was chosen as i) the study did not aim to investigate possible hemisphere-specific contributions to primary motor skills, but general methodological aspects in mapping primary motor functions and recovery, and as ii) this ensured high statistical power and adequate sample sizes for

multivariate lesion-behavior mapping. Figure 1 shows a topography of all normalized lesion maps.

CST lesion biomarkers

Following previous studies that computed CST lesion metrics to obtain biomarkers for post stroke motor outcome (Zhu et al. 2010; Feng et al., 2015; Findlater et al., 2019), variables 'CST load' and 'weighted CST load' were computed. Both metrics assess to what degree a structural lesion affects the CST by computing overlap metrics between a normalized lesion map and a probabilistic topography of the CST. The required probabilistic topography of the CST was taken from a publicly available white matter atlas based on diffusion tensor imaging data in 81 healthy subjects (Mori et al., 2008). This topography indicates for each voxel in imaging space a probability between 0 and 1 to belong to the CST. For 'CST load' (Zhu et al., 2010), the overlap between lesion map and the probabilistic CST map is weighted by a voxel's probability to be part of the CST. Accordingly, lesioned voxels that are more likely to be part of the CST contribute more to the CST lesion metric. For 'weighted CST load' (Zhu et al., 2010), the overlap between lesion map and the probabilistic CST map is weighted by the probability of a voxel to be part of the CST, and each voxel's contribution is weighted by the cross-sectional area of the CST on each axial slice of the brain atlas. Accordingly, lesioned voxels in dense parts of the CST fiber bundle contribute more to the CST lesion metric. Computations were performed in MATLAB 2019b using SPM 12 algorithms. For more details on CST lesion metrics, see the formulas in Zhu et al. (2010) and the current study's documented scripts, as available in the online materials.

To ensure that topographical signal strength, as assessed by maximum Z values in the univariate lesion behavior mapping analysis, is comparable between upper limb paresis (acute paresis max Z = 6.77; chronic paresis max Z = 6.58) and CST biomarkers (CST load max Z = 8.25; weighted CST load max Z = 8.18), random noise was added similar as in recent studies (Pustina et al., 2018). Noisy CST biomarkers were created by choosing a noise factor n in the range $0 < n < 1$ and calculating noisy biomarkers $nCST_{bm}$ based on original biomarkers CST_{bm} and uniform random values between 0 and 1 by $nCST_{bm} = n * CST_{bm} + (1 - n) * rand[0:1] * \max(CST_{bm})$. Factor n was tested in steps of 0.05 and manually chosen to provide optimal comparability between analyses of upper limb paresis and CST

lesion biomarkers. For more information, see the online materials of the present study. Maximum Z values for noisy CST biomarkers (CST load max Z = 6.92; weighted CST load max Z = 6.87) were comparable in signal strength to upper limb paresis. Note that both original and noisy CST lesion biomarkers were mapped and interpreted.

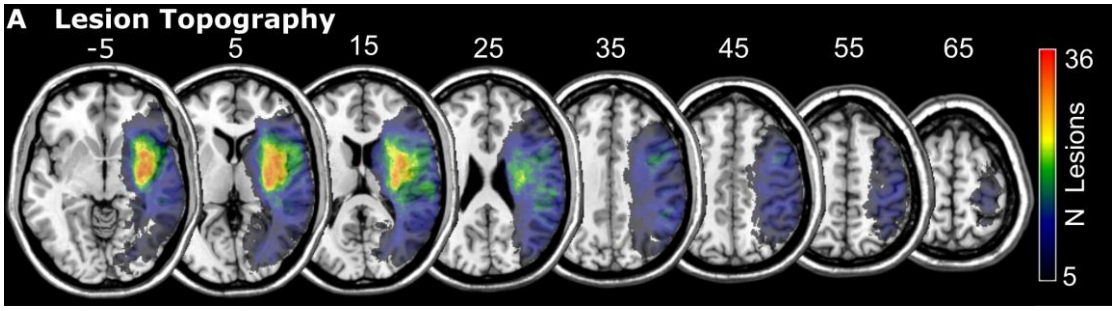

Figure 1: Lesion topography

Overlap topography of all 102 normalized binary lesion maps. The total number of overlapping lesions per voxel is depicted. Only voxels damaged in at least 5 patients are shown, which corresponds to the voxels included in the analyses. Numbers above slices indicate z-coordinates in MNI space.

Lesion behavior mapping

The relation between voxel-wise lesion status and motor variables was mapped by univariate voxel-based lesion behavior mapping (VLBM) and multivariate lesion behavior mapping (MLBM). All analyses were conducted at p = 0.05 only including voxels affected in at least five patients. VLBM was performed with voxel-wise general linear models, in the current study equivalent to t-tests, to investigate the relation between a voxel's binary lesion status and the behavioral target variable in NiiStat (https://www.nitrc.org/projects/niistat/). Family-wise error correction for multiple comparisons was applied by maximum statistic permutation thresholding with 1,000 permutations. MLBM was performed with support vector regression-based lesion symptom mapping (SVR-LSM; Zhang et al., 2014). Contrary to the typical procedures chosen in previous brain mapping studies using SVR-LSM (Zhang et al., 2014; Sperber et al., 2019), the present study aimed at a high comparability with prediction studies that directly utilized voxel-wise lesion data to predict the target variable (e.g. Rondina et al., 2016). Therefore, contrary to procedures common to mapping the functional architecture of the brain (Zhang et al., 2014; DeMarco &

Turkeltaub, 2018; Sperber et al., 2019), lesion data were not controlled for lesion size, and a support vector regression (SVR) with linear kernel and hyperparameter $C = 2^{-16}$ (Sperber, 2020) was used in libSVM (Chang & Lin, 2011). This allowed investigating which areas in the brain provide information that is utilized by a high-dimensional algorithm to model hemiparesis. Topographies controlled for lesion size are included in the online material. The contribution of each voxel's data to the model was assessed by computing the linear feature weights. Topographical inference was carried out by a permutation approach which re-computed the SVR with the same imaging data and permuted behavioral data 5000 times. Voxel-wise statistical significance was then assigned by comparison of the true feature weights with the permutation-derived feature weights. The resulting statistical topography was corrected by false discovery rate (FDR, Bejamini & Yekutieli, 2001) at $q = 0.05$. Largest clusters in the topographical statistical results were assigned to brain regions by reference to the AAL atlas and a selection of fiber tracts found in the JHU white matter atlas in mricron (https://www.nitrc.org/projects/mricron) and the probabilistic map of the CST (Mori et al., 2008). For detailed descriptive data and underlying topographies, see the online materials.

Data availability

Online materials including all analysis scripts, descriptive data, and resulting topographies are publicly available at http://dx.doi.org/10.17632/2pj8nxwbxr.1. The clinical datasets analyzed in the current study are not publicly available due to the data protection agreement approved by the local ethics committee and signed by the participants. They are available from Hans-Otto Karnath (karnath@uni-tuebingen.de) on reasonable request.

RESULTS

Neural correlates of upper limb paresis

Mapping the neural correlates of acute upper limb paresis with VLBM (Figure 2A) found significant voxels centered on the CST, but also extending beyond the CST into insula, putamen, rolandic (fronto-parietal) operculum, postcentral gyrus, superior temporal gyrus, hippocampus, external capsule, corona radiata, and superior longitudinal fasciculus. The results for MLBM (Figure 2B) even extended much further into many areas of the middle cerebral artery territory including frontal,

temporal, and parietal areas. Note that larger clusters were expected here, as MLBM was not controlled for lesion size and, contrary to VLBM, corrected by more liberal FDR correction.

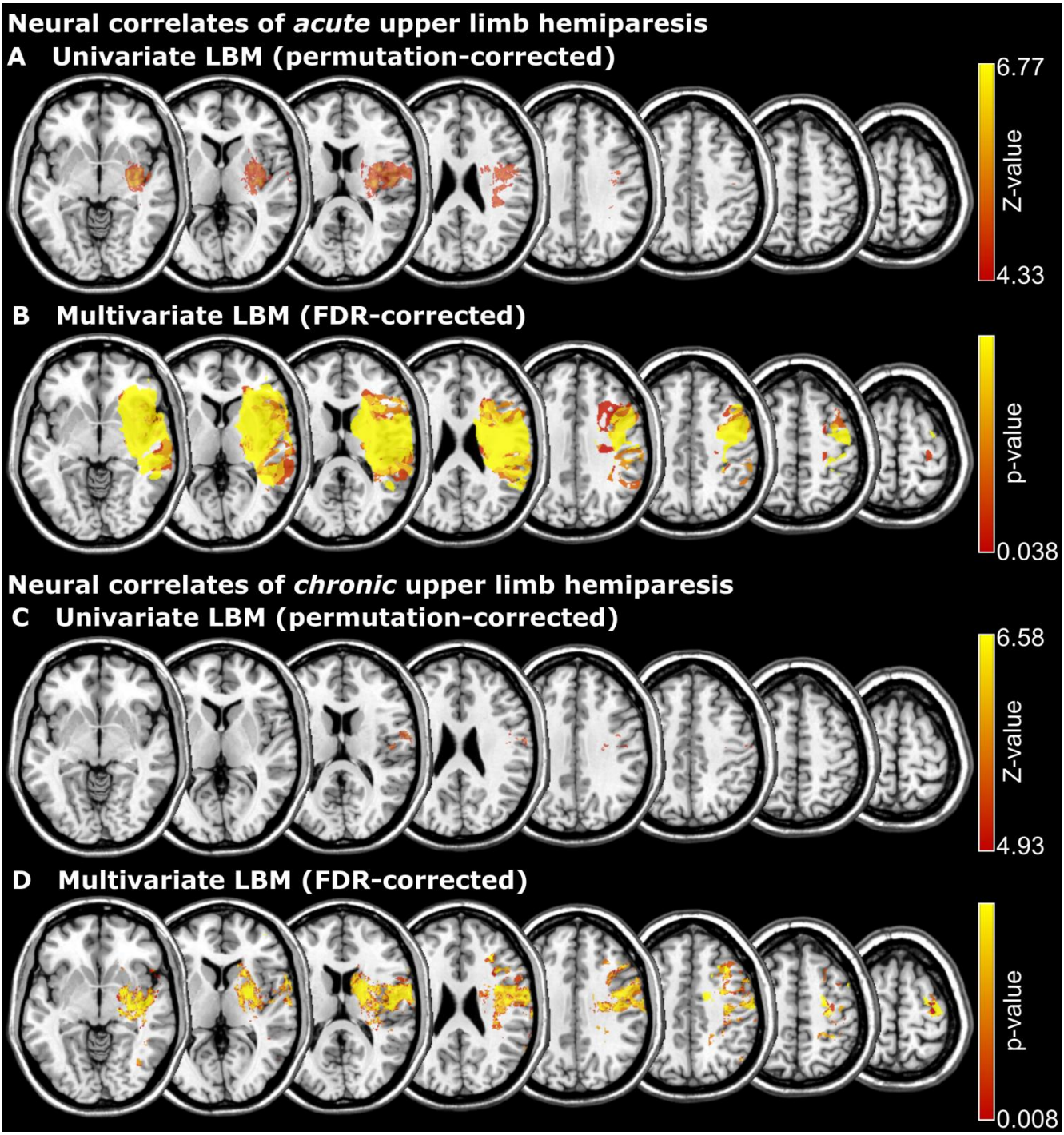

Figure 2: Lesion mapping of upper limb paresis

Voxel-wise lesion behavior mapping of upper limb paresis both for A) + B) acute and C) + D) chronic motor assessment. Note that, in the current study, multivariate lesion behavior mapping was intentionally not utilized following current standard

procedures for human brain mapping, and therefore univariate and multivariate methods cannot be directly compared.

Mapping chronic upper limb paresis with VLBM (Figure 2C), no significant results were located in the CST. Instead, small clusters were found located in post- and precentral gyrus, and rolandic operculum. Using MLBM (Figure 2D), results included the CST, and further pre- and postcentral gyri, inferior and middle frontal gyrus, rolandic operculum, hippocampus, caudatum, putamen, pallidum, superior temporal gyrus, and external capsule.

Neural correlates of CST lesion biomarkers

Mapping the neural correlates of 'CST load' without noise using VLBM (Figure 3A) found significant cluster in the CST, but also extending into pre- and post-central gyri, inferior, middle, and superior frontal gyri, supramarginal gyrus, rolandic operculum, superior temporal gyrus, putamen, pallidum, thalamus, superior longitudinal fasciculus, and corona radiata. For MLBM of 'CST load' without noise (Figure 3B), also features in the CST were significant, and additionally features in pre- and post-central gyri, middle frontal gyrus, supramarginal gyrus, rolandic operculum, superior temporal gyrus, putamen, pallidum, caudatum, thalamus, superior longitudinal fasciculus, and corona radiata.

Mapping the neural correlates of CST load with noise found, as expected, less significant voxels, due to reduced signal. Using VLBM (Figure 3C), significant voxels were found in pre- and postcentral gyrus, rolandic operculum, putamen, supramarginal gyrus, external capsule, corona radiata, and superior longitudinal fascicle. Using MLBM (Figure 3D), CST lesion load with noise was associated with damage in pre- and postcentral gyrus, rolandic operculum, putamen, pallidum, superior temporal gyrus, caudatum, hippocampus, supramarginal gyrus, thalamus, external capsule, corona radiata, and superior longitudinal fascicle.

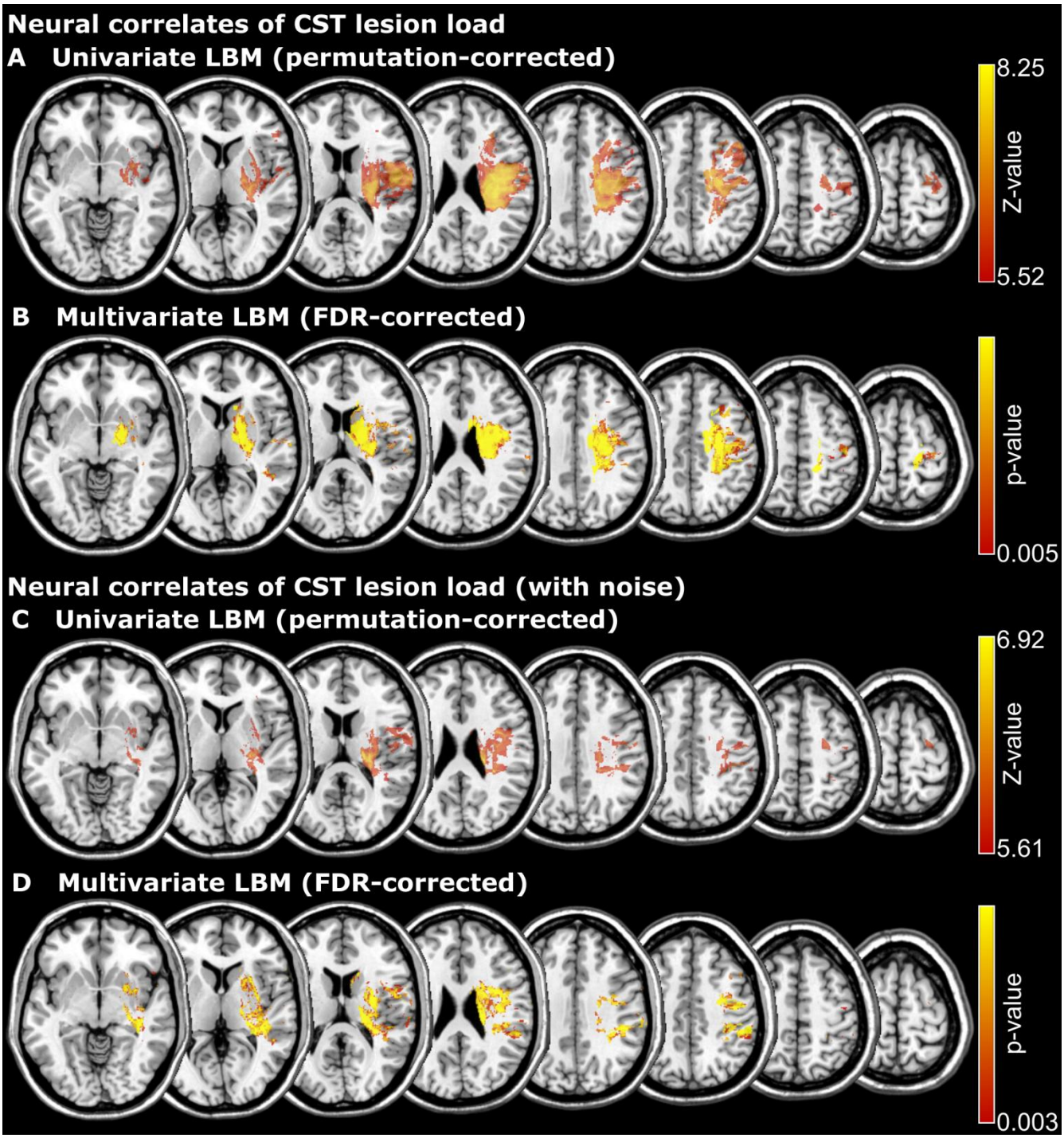

Figure 3: Lesion mapping of CST load

Voxel-wise lesion behavior mapping of CST load both for A) + B) raw lesion load scores and C) + D) lesion load scores with noise added to match peak statistical signal with the mapping of upper limb paresis scores.

Results for weighted CST load (supplementary Figure 1) closely resembled results for CST load and were thus not consulted in the data interpretation process. Topographies can be found in the supplementary and in the online materials of the

present study.

Next, topographies of upper limb paresis and CST lesion biomarkers were directly compared. First, univariate VLBM topographies of acute upper limb paresis and CST load with noise were contrasted (Figure 4A), mirroring a possible design to map the human brain (Karnath & Rennig, 2017). Several areas outside the CST were found to be associated with both variables, including rolandic operculum, putamen, external capsule, superior longitudinal fascicle, and corona radiata. Second, multivariate LBM topographies were compared between chronic upper limb paresis and CST load with noise (Figure 4B). In the current study, multivariate LBM assessed each voxel's predictive value in a high-dimensional multivariate model, identifying areas with a potential informative value in long-term outcome prediction. Again, several areas outside the CST were found to be associated with both variables, including rolandic operculum, putamen, pre- and postcentral gyri, hippocampus, external capsule, superior longitudinal fascicle, and corona radiata.

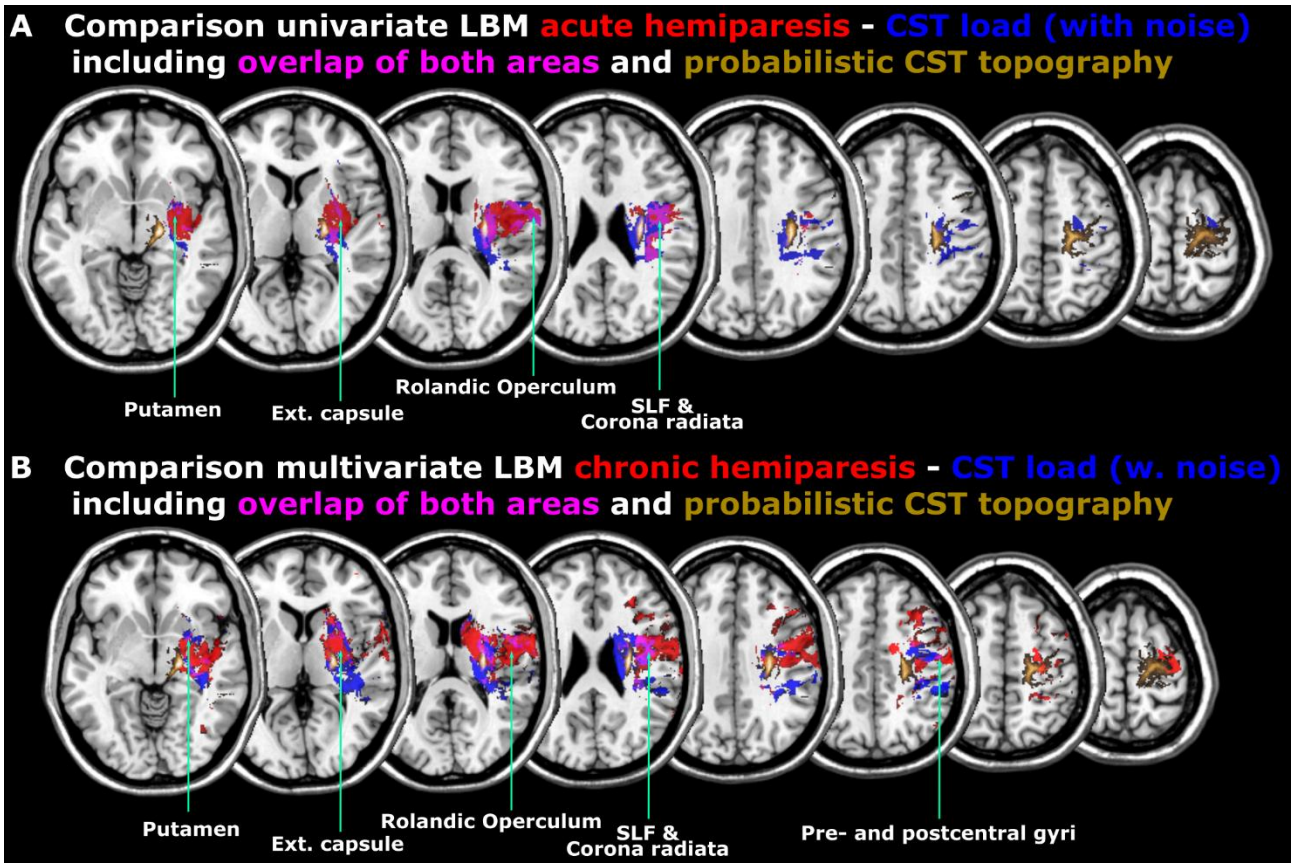

Figure 4: Comparison of the neural correlates of upper limb paresis and CST load

Direct comparison of statistical topographies in relation to the probabilistic topography of the CST. A) Comparison of univariate VLBM between acute upper limb paresis and CST load (with noise). B) Comparison of MLBM between chronic upper limb paresis and CST load (with noise). Areas of overlap are indicated and labeled. SLF = superior longitudinal fascicle

DISCUSSION

We mapped the neural correlates of upper limb paresis and of CST lesion biomarkers. The latter, per definition, only represent damage to the CST. In all mapping analyses of acute or chronic upper limb paresis, areas outside of the primary motor system were revealed. This could suggest that upper limb paresis is not only caused by damage to the primary motor system, but also by damage to additional brain areas. However, mapping CST lesion biomarkers also implicated several areas outside of the CST, with some correspondence to the areas implicated in upper limb paresis. Lesion information from these areas also significantly contributed to high-dimensional models for long-term motor outcome. Damage to these areas might not play a causal role in hemiparesis, while still providing predictive value for post-stroke motor outcome. These findings impose the need to rethink feature selection strategies in post-stroke outcome prediction based on imaging data.

At first, it might appear counter-intuitive that CST lesion biomarkers are related to damage to areas outside of the CST. This finding is based on the systematic complexity of brain lesions. Stroke follows the vasculature, resulting in typical stroke patterns, and neighboring brain regions are systematically damaged together. Thus, even if upper limb paresis was caused only by damage to primary motor regions, mapping hemiparesis would implicate areas outside of the primary motor system. This caveat of all current lesion-deficit inference methods has been acknowledged recently (Mah et al., 2014; Sperber et al., 2019; Sperber 2020). Notably, these areas outside of the primary motor system are predictive of hemiparesis, even if they are not directly causally related. In general, predictions can be made based on variables that are not the direct cause of the target variable: we can predict the weather from a swallow's flight, even though it is not the swallow that causes rain.

Several previous studies suggested that features taken from regions outside of the primary motor system should be included in post-stroke outcome prediction (Park et al., 2016; Rondina et al., 2016; Rondina et al., 2017). The rationale behind this approach was theories that causally link these regions and primary motor deficits, e.g.

the assumption that these areas are relevant for motor and sensory function (Rondina et al., 2016; Rondina et al., 2017). Indeed, prediction performance was improved by this strategy, but the present study suggests that this might have happened for other reasons. Some of the proposed motor regions overlapped with regions that were found to be associated with CST biomarkers in the present study, including subcortical and frontal regions. Notably, several of the proposed motor areas were not found to be related to motor deficits in the present study, and thus likely only a subset of the proposed motor regions underlay the improvement in prediction. The question remains which areas outside of the primary motor system actually play a causal role in primary motor deficits, and if this was the case for at least some of the regions chosen by previous prediction studies.

Conclusions

The current study was not designed to identify what areas constitute the true neural correlates of upper limb paresis. It rather implies that topographical results have to be interpreted with caution, and favors the view that the combination of lesion-deficit inference with strong hypotheses and behavioral experiments (Rinne et al., 2017), or other imaging and neurostimulation techniques is required to provide a solid foundation to understand the architecture of the human motor system and the human brain in general (Rorden & Karnath, 2004).

Post-stroke outcome prediction based on clinical imaging has potential to revolutionize individual patient care. Clinical imaging is part of any diagnostic protocol, and algorithms using only such data would be widely applicable and economic. However, no effective algorithms exist yet (Nachev et al., 2019). Low-dimensional prediction algorithms, such as simple linear regression, achieve up to moderate prediction performance at best based on CST lesion biomarkers (Findlater et al., 2019). For clinically useful algorithms, prediction performance has to be further improved, and high-dimensional models will likely be required to achieve this (Nachev et al., 2019). Feature selection is a vital step in any such algorithm based on machine learning. The current study indicates that this is a difficult task in stroke imaging data, which are highly complex and inter-related. Choosing features based on our understanding of the brain might perform sub-optimally, even for – compared to the complex language or spatial attention systems – relatively well-understood and more easily accessible brain functions such as primary motor abilities. Instead, data-

driven feature selection strategies might be required to improve prediction algorithms and bring us closer to effective predictive personalized medicine.

Declaration of Conflicting Interests

The authors declare that there is no conflict of interest.

Funding

The authors disclosed receipt of the following financial support for the research, authorship, and/or publication of this article: This work was supported by the German Research Foundation (KA 1258/23-1).

References

Buch, E.R., Rizk, S., Nicolo, P., Cohen, L.G., Schnider, A., Guggisberg, A.G., 2016. Predicting motor improvement after stroke with clinical assessment and diffusion tensor imaging. Neurology 86, 1924–5. https://doi.org/10.1212/WNL.0000000000002675

Chang, C., Lin, C., 2011. LIBSVM: A Library for Support Vector Machines. ACM Trans. Intell. Syst. Technol. 2, 1–27. https://doi.org/10.1145/1961189.1961199

DeMarco, A.T., Turkeltaub, P.E., 2018. A multivariate lesion symptom mapping toolbox and examination of lesion-volume biases and correction methods in lesion-symptom mapping. Hum. Brain Mapp. 39, 4169–4182. https://doi.org/10.1002/hbm.24289

Feng, W., Wang, J., Chhatbar, P.Y., Doughty, C., Landsittel, D., Lioutas, V.-A., Kautz, S., Schlaug, G., 2015. Corticospinal tract lesion load - A potential imaging biomarker for stroke motor outcomes. Ann. Neurol. https://doi.org/10.1002/ana.24510

Findlater, S.E., Hawe, R.L., Mazerolle, E.L., Al Sultan, A.S., Cassidy, J.M., Scott, S.H., Pike, G.B., Dukelow, S.P., 2019. Comparing CST Lesion Metrics as Biomarkers for Recovery of Motor and Proprioceptive Impairments After Stroke. Neurorehabil. Neural Repair 33, 848–861. https://doi.org/10.1177/1545968319868714

Frenkel-Toledo, S., Fridberg, G., Ofir, S., Bartur, G., Lowenthal-Raz, J., Granot, O., Handelzalts, S., Soroker, N., 2019. Lesion location impact on functional recovery of the hemiparetic upper limb. PLoS One 14, e0219738. https://doi.org/10.1371/journal.pone.0219738

Karnath, H.-O., Rennig, J., 2017. Investigating structure and function in the healthy human brain: validity of acute versus chronic lesion-symptom mapping. Brain Struct. Funct. 222, 2059–2070. https://doi.org/10.1007/s00429-016-1325-7

Lindenberg, R., Renga, V., Zhu, L.L., Betzler, F., Alsop, D., Schlaug, G., 2010. Structural integrity of corticospinal motor fibers predicts motor impairment in chronic stroke. Neurology 74, 280–287. https://doi.org/10.1212/WNL.0b013e3181ccc6d9

Lo, R., Gitelman, D., Levy, R., Hulvershorn, J., Parrish, T., 2010. Identification of critical areas for motor function recovery in chronic stroke subjects using voxel-based lesion symptom mapping. Neuroimage 49, 9–18. https://doi.org/10.1016/j.neuroimage.2009.08.044

Mah, Y.-H., Husain, M., Rees, G., Nachev, P., 2014. Human brain lesion-deficit inference remapped. Brain 137, 2522–31. https://doi.org/10.1093/brain/awu164

Mori, S., Oishi, K., Jiang, H., Jiang, L., Li, X., Akhter, K., Hua, K., Faria, A. V., Mahmood, A., Woods, R., Toga, A.W., Pike, G.B., Neto, P.R., Evans, A., Zhang, J., Huang, H., Miller, M.I., van Zijl, P., Mazziotta, J., 2008. Stereotaxic

white matter atlas based on diffusion tensor imaging in an ICBM template. Neuroimage 40, 570–582. https://doi.org/10.1016/j.neuroimage.2007.12.035

Nachev, P., Rees, G., Frackowiak, R., 2018. Lost in translation. F1000Research 7, 620. https://doi.org/10.12688/f1000research.15020.1

Park, C.H., Kou, N., Ward, N.S., 2016. The contribution of lesion location to upper limb deficit after stroke. J. Neurol. Neurosurg. Psychiatry 87, 1283–1286. https://doi.org/10.1136/jnnp-2015-312738

Pustina, D., Avants, B., Faseyitan, O.K., Medaglia, J.D., Coslett, H.B., 2018. Improved accuracy of lesion to symptom mapping with multivariate sparse canonical correlations. Neuropsychologia 115, 154–166. https://doi.org/10.1016/j.neuropsychologia.2017.08.027

Rinne, P., Hassan, M., Fernandes, C., Han, E., Hennessy, E., Waldman, A., Sharma, P., Soto, D., Leech, R., Malhotra, P.A., Bentley, P., 2017. Motor dexterity and strength depend upon integrity of the attention-control system. Proc. Natl. Acad. Sci. 201715617. https://doi.org/10.1073/pnas.1715617115

Rondina, J.M., Filippone, M., Girolami, M., Ward, N.S., 2016. Decoding post-stroke motor function from structural brain imaging. NeuroImage Clin. 12, 372–380. https://doi.org/10.1016/j.nicl.2016.07.014

Rondina, J.M., Park, C., Ward, N.S., 2017. Brain regions important for recovery after severe post-stroke upper limb paresis. J. Neurol. Neurosurg. Psychiatry 88, 737–743. https://doi.org/10.1136/jnnp-2016-315030

Rorden, C., Karnath, H.O., 2004. Using human brain lesions to infer function: A relic from a past era in the fMRI age? Nat. Rev. Neurosci. 5, 812–819. https://doi.org/10.1038/nrn1521

Rorden, C., Bonilha, L., Fridriksson, J., Bender, B., Karnath, H.O., 2012. Age-specific CT and MRI templates for spatial normalization. Neuroimage 61, 957–965. https://doi.org/10.1016/j.neuroimage.2012.03.020

Sperber, C., 2020. Rethinking causality and data complexity in brain lesion-behaviour inference and its implications for lesion-behaviour modelling. Cortex 126, 49–62. https://doi.org/10.1016/j.cortex.2020.01.004

Sperber, C., Wiesen, D., Karnath, H.O., 2019. An empirical evaluation of multivariate lesion behaviour mapping using support vector regression. Hum. Brain Mapp. 40, 1381–1390. https://doi.org/10.1002/hbm.24476

Sterr, A., Dean, P.J. a., Szameitat, A.J., Conforto, A.B., Shen, S., 2014. Corticospinal Tract Integrity and Lesion Volume Play Different Roles in Chronic Hemiparesis and Its Improvement Through Motor Practice. Neurorehabil. Neural Repair 28, 335–343. https://doi.org/10.1177/1545968313510972

Stinear, C.M., Barber, P.A., Petoe, M., Anwar, S., Byblow, W.D., 2012. The PREP algorithm predicts potential for upper limb recovery after stroke. Brain 135, 2527–2535. https://doi.org/10.1093/brain/aws146

Wang, L.E., Tittgemeyer, M., Imperati, D., Diekhoff, S., Ameli, M., Fink, G.R., Grefkes, C., 2012. Degeneration of corpus callosum and recovery of motor function after stroke: A multimodal magnetic resonance imaging study. Hum. Brain Mapp. 33, 2941–2956. https://doi.org/10.1002/hbm.21417

Wenzelburger, R., 2005. Hand coordination following capsular stroke. Brain 128, 64–74. https://doi.org/10.1093/brain/awh317

Yekutieli, D., Benjamini, Y., 2001. The control of the false discovery rate in multiple testing under dependency. Ann. Stat. 29, 1165–1188. https://doi.org/10.1214/aos/1013699998

Zhang, Y., Kimberg, D.Y., Coslett, H.B., Schwartz, M.F., Wang, Z., 2014. Multivariate lesion-symptom mapping using support vector regression. Hum. Brain Mapp. 35, 5861–5876. https://doi.org/10.1002/hbm.22590

Zhu, L.L., Lindenberg, R., Alexander, M.P., Schlaug, G., 2010. Lesion load of the corticospinal tract predicts motor impairment in chronic stroke. Stroke. 41, 910–5. https://doi.org/10.1161/STROKEAHA.109.577023

Figure Legends

Figure 1: Lesion topography and corticospinal tract

Overlap topography of all 102 normalized binary lesion maps. The total number of overlapping lesions per voxel is depicted. Only voxels damaged in at least 5 patients are shown, which corresponds to the voxels included in the analyses. Numbers above slices indicate z-coordinates in MNI space.

Figure 2: Lesion mapping of upper limb paresis

Voxel-wise lesion behavior mapping of upper limb paresis both for A) + B) acute and C) + D) chronic motor assessment. Note that, in the current study, multivariate lesion behavior mapping was intentionally not utilized following current standard procedures for human brain mapping, and therefore univariate and multivariate methods cannot be directly compared.

Figure 3: Lesion mapping of CST load

Voxel-wise lesion behavior mapping of CST load both for A) + B) raw lesion load scores and C) + D) lesion load scores with noise added to match peak statistical signal with the mapping of upper limb paresis scores.

Figure 4: Comparison of the neural correlates of upper limb paresis and CST load

Direct comparison of statistical topographies in relation to the probabilistic topography of the CST. A) Comparison of univariate VLBM between acute upper limb paresis and CST load (with noise). B) Comparison of MLBM between chronic upper limb paresis and CST load (with noise). Areas of overlap are indicated and labeled. SLF = superior longitudinal fascicle

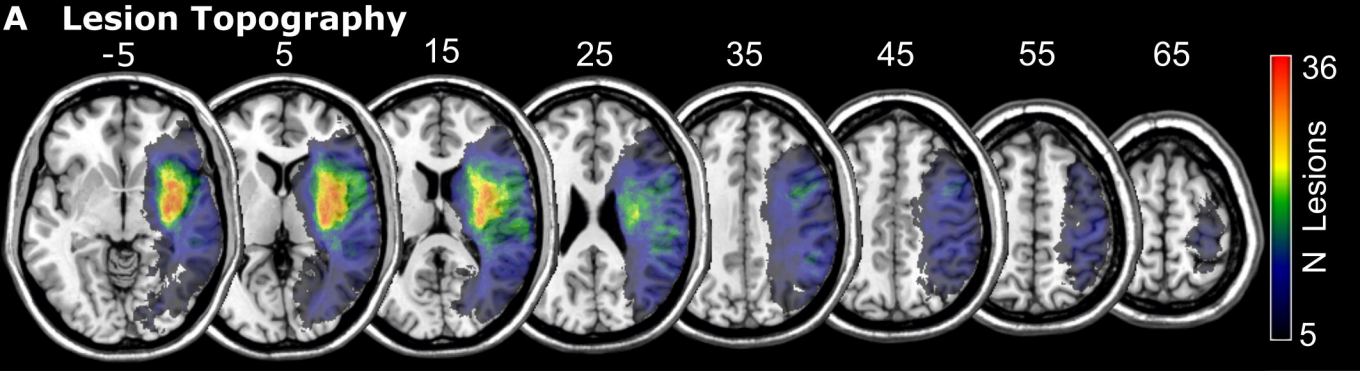
A Lesion Topography
-5
5
15
25
35
45
55
65
36
N Lesions
5

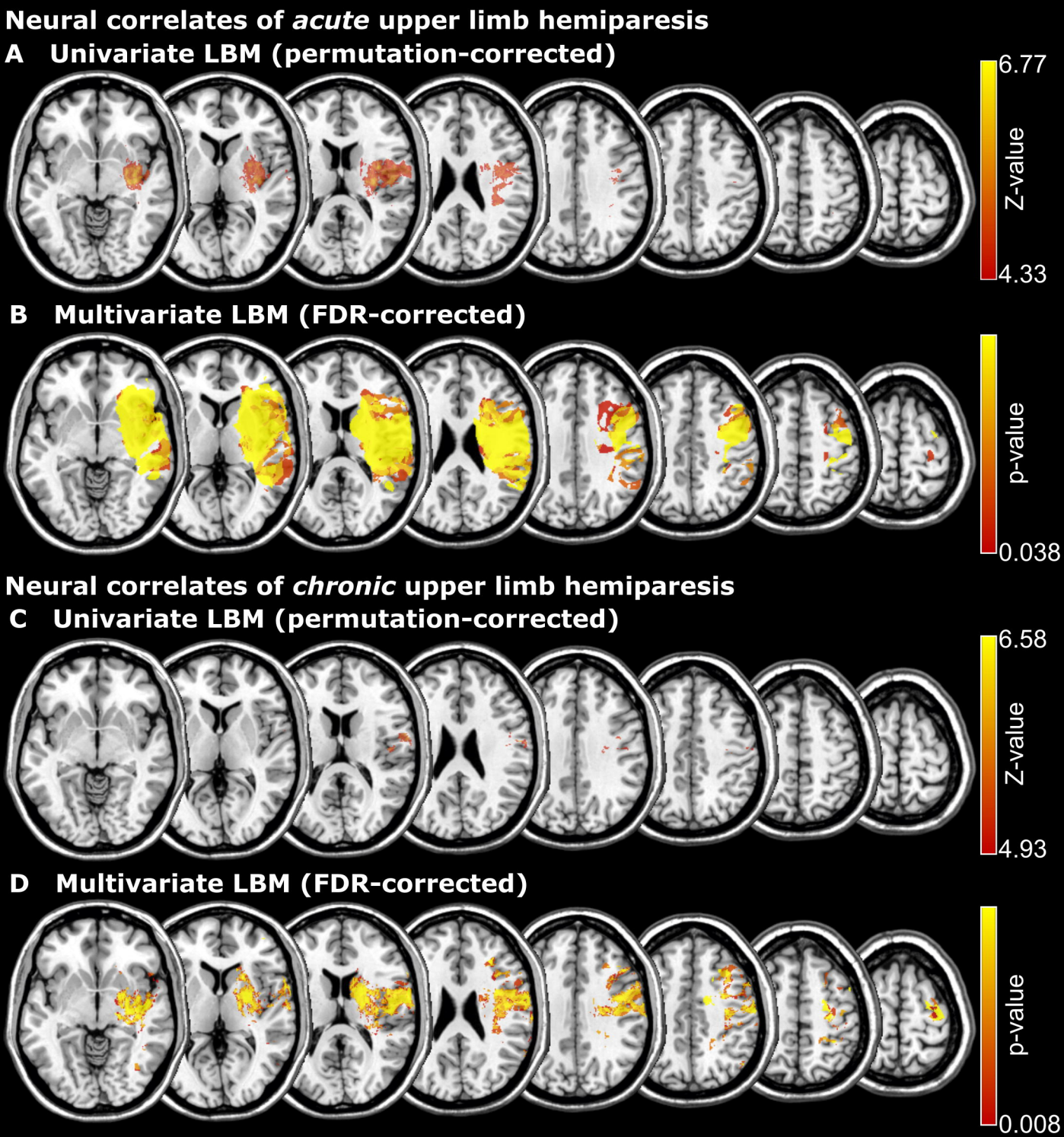
Neural correlates of *acute* upper limb hemiparesis
A Univariate LBM (permutation-corrected)
6.77
Z-value
4.33
B Multivariate LBM (FDR-corrected)
p-value
0.038
Neural correlates of *chronic* upper limb hemiparesis
C Univariate LBM (permutation-corrected)
6.58
Z-value
4.93
D Multivariate LBM (FDR-corrected)
p-value
0.008

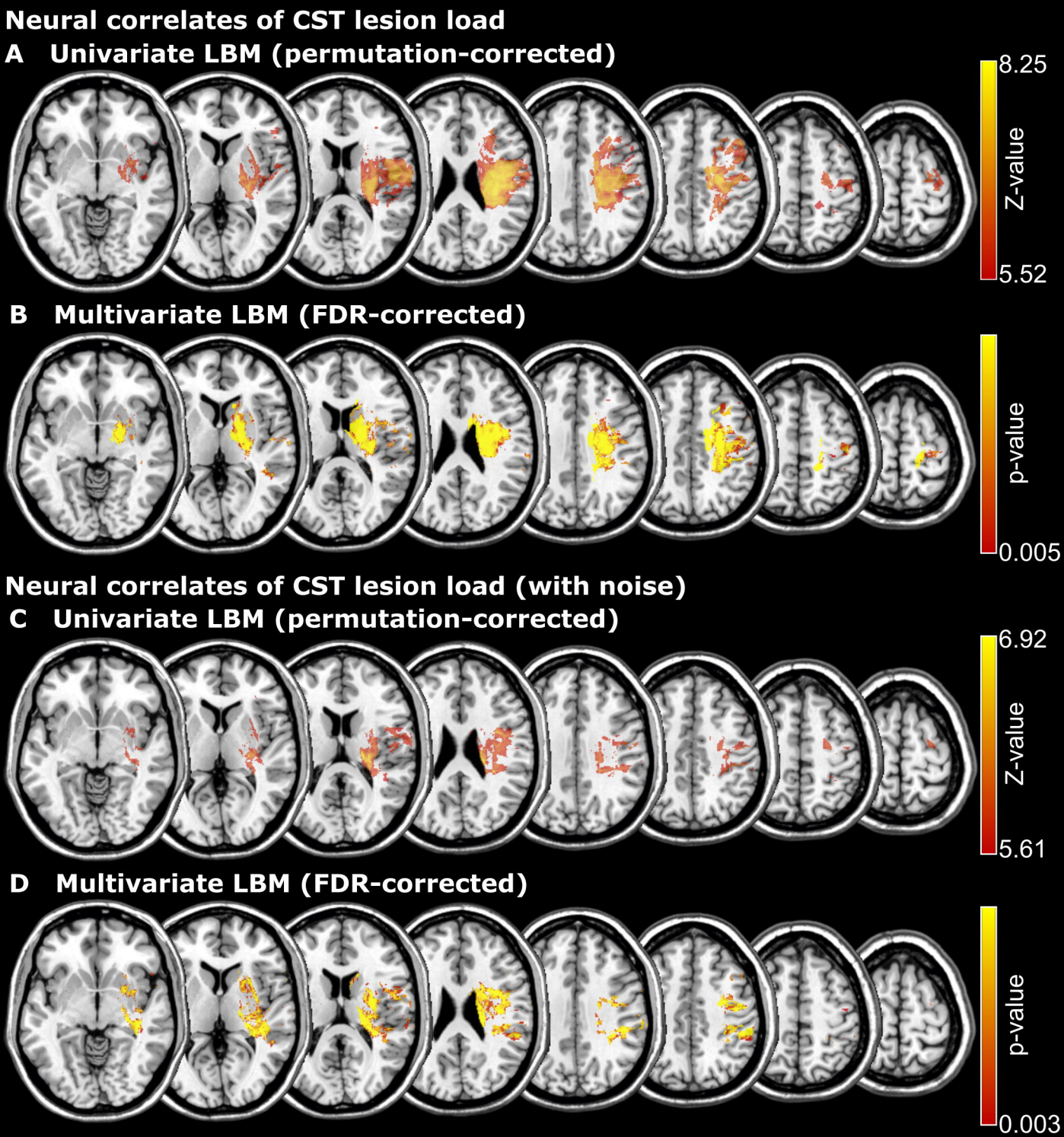
Neural correlates of CST lesion load
A Univariate LBM (permutation-corrected)
8.25
Z-value
5.52
B Multivariate LBM (FDR-corrected)
p-value
0.005
Neural correlates of CST lesion load (with noise)
C Univariate LBM (permutation-corrected)
6.92
Z-value
5.61
D Multivariate LBM (FDR-corrected)
p-value
0.003

A Comparison univariate LBM acute hemiparesis - CST load (with noise) including overlap of both areas and probabilistic CST topography

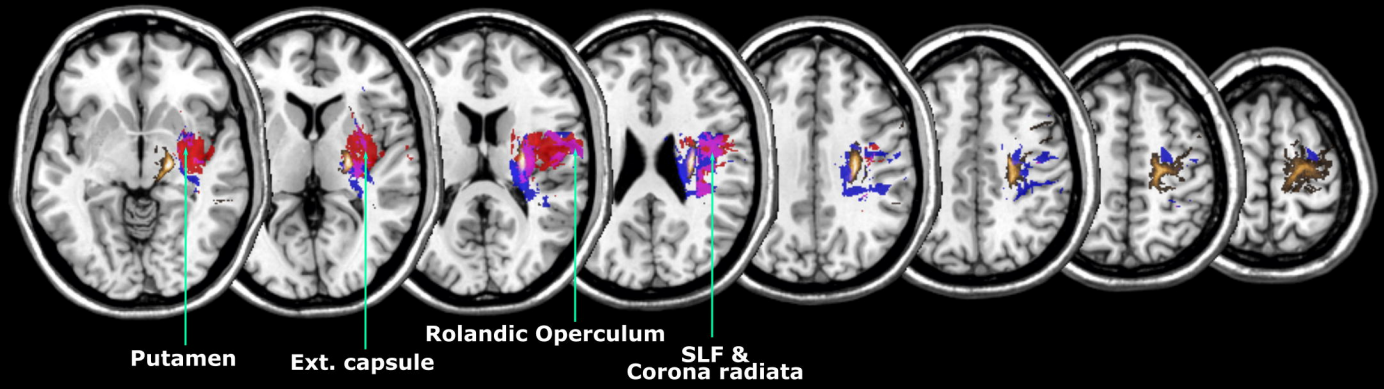
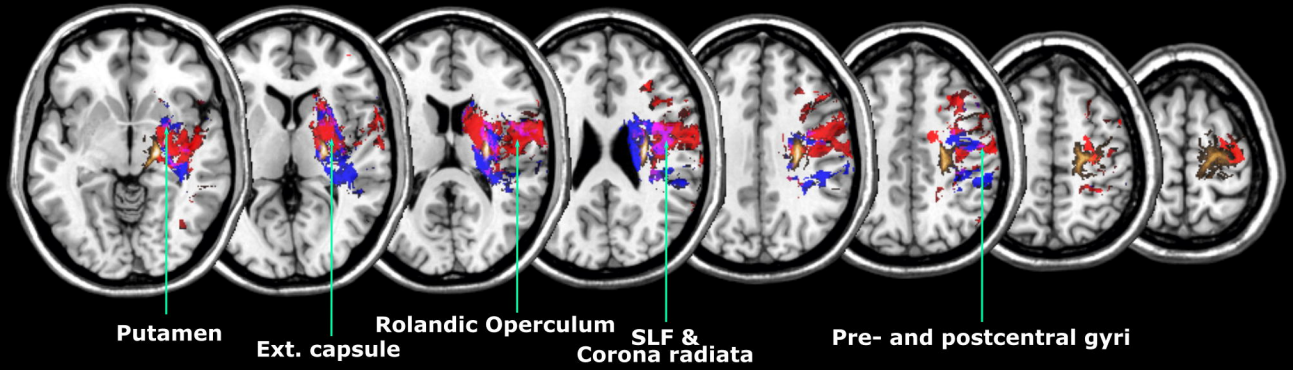
B Comparison multivariate LBM chronic hemiparesis - CST load (w. noise) including overlap of both areas and probabilistic CST topography